doi.org/10.36721/PJPS.2026.39.12.356.1

Compound Miao medicine Jiuxian Luohan bone-setting decoction improves rat femoral fracture healing: Associations with osteogenic and apoptosis-related markers

Haoran Wan[1], Zhengxing Xie[1], Lingcheng Deng[1], Liang Yu[1], Zhong Ning[1], Hongfa Wang[2], Jiabao Zheng[1], Shaoyang Zhai[1] and Lianghua Tang[3]*

[1]Guizhou University of Traditional Chinese Medicine, Guiyang, Guizhou, China
[2]Department of Orthopedics, Taijiang County People's Hospital, Taijiang, Guizhou, China
[3]Department of Joint Orthopedics, Second Affiliated Hospital of Guizhou University of Traditional Chinese Medicine, Guiyang, Guizhou, China

Abstract: **Background**: Fracture healing is a dynamic biological process involving inflammation, callus formation, mineralization and remodeling. Osteogenic and apoptosis-related markers may reflect changes during repair, but tissue-level marker expression alone does not establish a causal apoptotic mechanism. **Objectives**: To evaluate whether Compound Miao medicine Jiuxian Luohan bone-setting decoction is associated with improved femoral fracture healing in rats and with altered expression of runt-related transcription factor 2 (Runx2), Osterix, procollagen type I N-terminal propeptide (PINP), Bcl-2-associated X protein (Bax) and Caspase-3 at the fracture site. **Methods**: Twenty-five male specific-pathogen-free (SPF) Sprague-Dawley rats were used to establish a right femoral fracture model and were randomized into five groups (n=5/group): model, low-, medium- and high-dose decoction and orthopedic bone-setting tablet groups. Treatments were initiated 24 h after modeling and administered by gavage twice daily for 30 days. Anteroposterior and lateral radiographs were obtained on day 15 and scored using the Lane-Sandhu system. Fracture-site tissues were collected on day 30 for reverse transcription quantitative polymerase chain reaction (RT-qPCR), Western blotting, immunohistochemistry and Alizarin Red staining. **Results**: Compared with the model group, the high-dose decoction group showed a higher Lane-Sandhu score at week 2 and greater callus formation. Runx2, Osterix and PINP mRNA/protein levels increased, whereas Bax and Caspase-3 mRNA/protein levels decreased in treated groups, particularly in the high-dose group. Alizarin Red staining indicated greater deposition of mineralized matrix in treated tissues. **Conclusion**: Compound Miao medicine Jiuxian Luohan bone-setting decoction was associated with improved radiographic healing and favorable changes in osteogenic and apoptosis-related markers in this rat femoral fracture model.

Keywords: Bax; Caspase-3; Compound Miao medicine Jiuxian Luohan bone-setting decoction; Femoral fracture; Osterix; PINP; Runx2; Rat model

Submitted on 05-06-2026 – Revised on 15-07-2026 – Accepted on 04-08-2026 – Available online on 05-09-2026 – Published on 01-12-2026

INTRODUCTION

Fractures commonly result from mechanical trauma and can cause deformity, swelling, pain, bleeding, functional limitation and disability. Fracture repair progresses through overlapping inflammatory, reparative, mineralization and remodeling phases. Although surgical fixation and postoperative rehabilitation are routinely used, delayed union and nonunion remain clinically important complications that increase treatment burden, prolong pain and may necessitate secondary procedures (Einhorn and Gerstenfeld, 2015; Bahney *et al*., 2019).

Osteoblast proliferation, differentiation, extracellular-matrix maturation, mineralization and survival are central to callus formation and bone regeneration. Impaired osteoblast differentiation or excessive cell death may disrupt the balance between bone formation and resorption, thereby delaying healing. Runx2 and Osterix are key transcriptional regulators of osteoblast differentiation, whereas PINP reflects type I collagen synthesis and bone formation (Ponzetti and Rucci, 2021; Chan *et al*., 2021; Qin *et al*., 2021). Bax and Caspase-3 are apoptosis-related markers; however, changes in their expression represent indirect evidence of apoptosis unless confirmed by direct apoptosis assays (Obeng, 2021; Sahoo *et al*., 2023). Compound Miao medicine Jiuxian Luohan bone-setting decoction is based on the Miao medicine concepts of "expelling toxins," "tonifying the kidney," and "promoting blood circulation." Experimental studies in rat fracture models have demonstrated that local biological cues can influence callus formation and bone regeneration (Zhang *et al*., 2016). The present study therefore investigated whether Jiuxian Luohan bone-setting decoction was associated with fracture healing and with changes in osteogenic and apoptosis-related molecular markers in a rat femoral fracture model. As an animal experiment, the findings should be interpreted as preclinical evidence requiring further mechanistic and translational validation.

MATERIALS AND METHODS

Study design and ethical statement

This was a controlled *in-vivo* experimental animal study using a rat femoral fracture model. All animal procedures

**Corresponding author:* e-mail: tlh202606@163.com

were approved by the Animal Ethics Committee of Guizhou University of Traditional Chinese Medicine (approval no. 2024005). The study was reported in accordance with the ARRIVE 2.0 guidelines (Percie du Sert *et al*., 2020).

Experimental animals

Twenty-five male specific-pathogen-free (SPF) Sprague-Dawley rats, aged 7-8 weeks and weighing 180-220 g, were obtained from Henan Skebes Biotechnology Co., Ltd. (Animal Production License No. SCXK [Yu] 2020-005). Male rats were used to reduce variability in hormonal cycles. The absence of female animals is addressed in the limitations section. Rats were acclimatized for 1 week before modeling and housed under controlled conditions (22 ± 2°C, 50%-60% relative humidity, 12-h light/dark cycle), with free access to standard laboratory chow and sterile drinking water.

Drugs and primary reagents

The verified formula of Compound Miao medicine Jiuxian Luohan bone-setting decoction was standardized as follows: Dihuang (Rehmannia glutinosa) 20 g, Xiantao Cao (Scutellaria baicalensis) 20 g, Jiujie Cha (Cynanchum wilfordii) 20 g, Sanqi (Panax notoginseng) 9 g, Ziran Tong (Pyritum) 9 g, Xuduan (Dipsacus asper) 9 g, Duzhong (Eucommia ulmoides) 12 g, Heshouwu (Polygonum multiflorum) 12 g and Yinyanghuo (Epimedium sagittatum) 12 g. All herbs were supplied by the Chinese Medicine Pharmacy of the Second Affiliated Hospital of Guizhou University of Traditional Chinese Medicine. Herbs were steeped in 1000 mL sterile distilled water for 1 h and decocted for 30 min; 500 mL sterile distilled water was then added for a second 30-min decoction. The two decoctions were combined, filtered and concentrated to the required gavage concentrations. Aliquots were stored at 4°C for short-term use within 48 h; for longer storage, aliquots were kept at -20°C and protected from repeated freeze-thaw cycles. Orthopedic bone-setting tablets (batch no. 20230367; Dalian Meiluo Traditional Chinese Medicine Factory Co., Ltd.) were used as the positive-control medication. Tablets were suspended in sterile distilled water to prepare the administration suspension.

PCR primers were purchased from Yingwei Jieji; the total RNA extraction kit was purchased from Tiangen; the reverse-transcription kit was purchased from Novozymes; the Western protein marker (Servicebio G2086), protein lysis buffer (Youke Zhuoye Bio P001), bicinchoninic acid (BCA) protein assay kit (CWBio 02912E), hematoxylin stain (Wuhan Siver), xylene (Sinopharm Chemical Reagent Co., Ltd.) and Alizarin Red S stain (Servicebio) were purchased from the stated suppliers. All commercial kits and reagents were used according to the manufacturers' instructions unless otherwise specified.

Major instruments

Major instruments included a CFX96 real-time fluorescence quantitative PCR instrument (Bio-Rad), 5810R desktop high-speed refrigerated centrifuge (Eppendorf), Mini Pro 300V power-supply electrophoresis unit (Major Science), Sub-System 70 electrophoresis tank (Labnet Inc.), MX-F vortex mixer (Wuhan Saivell) and BLX-5 mini dental X-ray unit (Zhengzhou Tianjie).

Establishment of the femoral fracture model

After one week of acclimatization, the femoral fracture model was established with minor modifications, following a previously described method (Hou *et al*., 2021). Rats were anesthetized with inhaled isoflurane and placed in the left lateral recumbent position. The right hind limb was immobilized, the femur was palpated and marked, local hair was shaved and the surgical area was disinfected with iodine solution. A 1 cm incision was made along the marked line to the deep fascia. The muscles were bluntly dissected to expose the femur and the periosteum was incised and dissected. A 1.5-cm-diameter, 0.1-mm-thick saw blade mounted on an electric bone saw (ExampleMed Instruments Co., Ltd., China; Model ES-1000) was used to cut perpendicular to the longitudinal axis of the femur at 1000 rpm under continuous saline irrigation until approximately one-half to two-thirds of the femoral cross-sectional thickness was reached. Two needle holders grasped opposite ends of the cut and the femur was fractured. A 1.5 mm diameter, 18-21 mm long Kirschner wire was inserted for intramedullary fixation. The incision was irrigated with saline and closed with layered sutures. Radiography confirmed fracture alignment and Kirschner-wire positioning.

Animal grouping, randomization, blinding and administration

The 25 rats were randomly allocated using a computer-generated random-number sequence into five groups (n=5 per group): model group, low-dose decoction group, medium-dose decoction group, high-dose decoction group and orthopedic bone-setting tablet group. Drug intervention commenced 24 h after successful modeling. The model group received an equivalent volume of 0.9% NaCl by gavage. The adult clinical daily dose of the decoction was 1.88 g/kg and rat-equivalent doses were calculated by body-surface-area conversion according to Xu Shuyun's pharmacological experimental methodology. The low-, medium- and high-dose groups received 2.95, 5.90 and 11.80 g/kg of concentrated decoction, respectively. The orthopedic bone-setting tablet group received 0.24 g/kg tablet suspension by gavage. All groups received twice-daily gavage for 30 consecutive days. Radiographic scoring, histological image analysis, immunohistochemistry quantification and Western blot densitometry were performed by investigators blinded to group allocation. Group codes were opened only after primary data extraction was completed. On day 15, radiographs of the modeled site were obtained to evaluate Kirschner-wire position and fracture-healing progress. On day 30, rats were deeply anesthetized with sodium pentobarbital (50 mg/kg, intraperitoneally) before

euthanasia and bone tissue from the modeled fracture site was subsequently harvested. Samples for RNA and protein assays were snap-frozen in liquid nitrogen using a cryogenic storage tank (Thermo Fisher Scientific, USA; Model CY50985) and subsequently stored in an ultra-low-temperature freezer at −80° C (Thermo Fisher Scientific, USA; Model TSX60086A) until further analysis. Samples for histology, immunohistochemistry and Alizarin Red staining were fixed in 4% paraformaldehyde and processed for paraffin embedding after decalcification.

Radiographic examination and Lane-Sandhu scoring

At week 2 post-surgery, the right femur of each rat was examined by X-ray under anesthesia using the BLX-5 mini dental X-ray unit. Anteroposterior (AP) and mediolateral/lateral (ML/Lat) views were obtained. Fracture alignment, Kirschner-wire position, callus formation and fracture-line clarity were evaluated. Radiographic healing was graded using the 0-4 Lane-Sandhu scale: 0 = no visible callus or union; 1 = minimal callus with a clearly visible fracture line; 2 = moderate callus with partial cortical bridging; 3 = abundant bridging callus with incomplete remodeling; and 4 = complete union/remodeling. Accordingly, lower scores indicated absent or limited healing, whereas higher scores indicated more advanced callus bridging and union. Three orthopedic investigators, experienced in experimental fracture imaging and blinded to group allocation, independently scored each radiograph on two occasions, 1 week apart. For each rat, the six ratings (three assessors × two scoring sessions) were averaged to obtain the Lane-Sandhu score for the statistical analysis.

RT-qPCR detection of Runx2, Osterix, PINP, Bax and Caspase-3 mRNA expression

Total RNA was extracted from fracture-site bone tissue using the total RNA extraction kit according to the manufacturer's protocol. RNA concentration and purity were assessed by spectrophotometry and samples with A260/A280 ratios of 1.8-2.1 were used. Complementary DNA was synthesized using the reverse transcription kit. Quantitative real-time PCR was performed on a Bio-Rad CFX96 platform using SYBR Green chemistry in a 20 μL reaction system. Cycling conditions were: 95°C for 30 s; 40 cycles of 95°C for 5 s and 60°C for 30 s; followed by melt-curve analysis to verify single-product amplification. Each biological sample was run in triplicate technical reactions. ACTB was used as the reference gene and relative expression was calculated using the $2^{-\Delta\Delta Ct}$ method. Primer sequences are shown in table 1.

Western blot detection of Runx2, Osterix, PINP, Bax and Caspase-3 protein expression

Fracture-site tissue was lysed in pre-chilled Radio Immuno Precipitation Assay (RIPA) buffer supplemented with a protease inhibitor cocktail. Lysates were centrifuged at 13,000 rpm for 20 min at 4 °C using a 5810R desktop high-speed refrigerated centrifuge (Eppendorf, Germany) and the supernatants were subsequently collected, aliquoted and stored at −80°C until further analysis. Protein concentration was measured using the bicinchoninic acid (BCA) method. A standard curve was generated from serially diluted protein standards and absorbance at 562 nm was measured using a microplate reader (BioTek Instruments, USA; Model Epoch 2). Sample protein concentrations were calculated from the standard curve. Equal amounts of protein were denatured at 95° C for 5 min using a dry-block heater (Thermo Fisher Scientific, USA; Model Digital Dry Bath), separated by SDS-PAGE using a Mini Pro 300V power supply (Major Science, Taiwan, China) and a Sub-System 70 electrophoresis unit (Labnet International, USA) and subsequently transferred onto 0.45- μ m PVDF membranes using a wet-transfer apparatus (Bio-Rad Laboratories, USA; Model Mini Trans-Blot Cell) at a constant current of 300 mA for 90 min. The antibodies used in this study are shown in table 2.

Membranes were blocked in 5% bovine serum albumin (BSA) in Tris-buffered saline with Tween-20 (TBST) for 1 h at room temperature and incubated overnight at 4°C with primary antibodies against Runx2, Osterix, PINP, Bax, Caspase-3 and β-actin. After three 10-min washes with TBST, membranes were incubated with the appropriate horseradish-peroxidase-conjugated secondary antibody. Signals were developed by chemiluminescence and band intensities were quantified using ImageJ software. Target proteins were normalized to β-actin.

Immunohistochemical detection of Runx2, Osterix, PINP, Bax and Caspase-3 protein expression in fracture-site bone tissue

Paraffin-embedded fracture-site bone tissue sections were deparaffinized in xylene I, II and III for 15 min each, followed by anhydrous ethanol I and II for 5 min each, 85% ethanol for 5 min and 75% ethanol for 5 min. Sections were rinsed with distilled water, subjected to antigen retrieval, incubated to block endogenous peroxidase activity and blocked with serum. Sections were incubated with primary antibodies against Runx2, Osterix, PINP, Bax and Caspase-3, followed by incubation with secondary antibodies, DAB visualization, hematoxylin counterstaining, dehydration and mounting. Hematoxylin-stained nuclei appeared blue and DAB-positive staining appeared brown-yellow. For each animal, five non-overlapping high-power fields (×400) around the fracture callus region were analyzed. Images were captured using identical exposure settings. Quantification was performed with ImageJ by calculating the percentage of positively stained area or integrated optical density per field. Two blinded observers independently performed the analysis and the average value was used for statistical analysis.

Table 1: Primer information used in this study.

Gene	Forward sequence (5'-3')	Reverse sequence (5'-3')	PCR product (bp)
ACTB	CCTAGACTTCGAGCAAGAGA	GGAAGGAAGGCTGGAAGA	140
Caspase-3	ATGACGACAGGGTGCTACGA	TGAGGCTGCTGCATAATCG	114
Bax	AGGACGCATCCACCAAGAA	CAAAGTAGAAAAGGGCAACCAC	195
Runx2	CCTTCCCTCCGAGACCCTAA	ATGCAAATGCTCCCGCTACT	166
Osterix	GCCTACTTACCCGTCTGACTTT	GCCCACTATTGCCAACTGC	131
PINP	CGATTCACCTACAGCACGCTT	GGATGGAGGGAGTTTACACGAA	196

Table 2: The Western blot antibodies used in this study were purchased from the suppliers listed below and used according to the manufacturers' instructions after preliminary optimization of dilution conditions.

Antibody/reagent	Supplier	Catalog no.	Host/type	WB dilution
Anti-Runx2 primary antibody	Affinity biosciences	AF5186	Rabbit polyclonal	1:1000
Anti-Osterix/SP7 primary antibody	Affinity biosciences	DF7731	Rabbit polyclonal	1:1000
Anti-PINP/P1NP primary antibody	Invitrogen/Thermo fisher scientific	PA5-35379	Rabbit polyclonal	1:1000
Anti-Bax primary antibody	Affinity biosciences	AF0120	Rabbit polyclonal	1:1000
Anti-Caspase-3 primary antibody	Affinity biosciences	AF6311	Rabbit polyclonal	1:1000
Anti-beta-actin loading-control antibody	Affinity biosciences	AF7018	Rabbit polyclonal	1:5000
HRP-conjugated goat anti-rabbit IgG secondary antibody	Affinity biosciences	S0001	Secondary antibody	1:5000

Antibodies were stored at -20°C or 4°C according to the product datasheets and protected from repeated freeze-thaw cycles.

Alizarin red staining of fracture-site bone tissue

Alizarin Red staining was performed on decalcified fracture-site tissue sections rather than cultured cells; therefore, calcified nodules were not counted. Paraffin sections were deparaffinized, rehydrated, rinsed with phosphate-buffered saline (PBS) and stained with Alizarin Red S solution for 30 min at room temperature. After washing with PBS, the sections were examined using a light microscope (Olympus Corporation, Tokyo, Japan; Model BX53) and representative images were captured using a digital microscope camera (Olympus Corporation, Tokyo, Japan; Model DP74). For each animal, five non-overlapping, randomly selected fields per section were analyzed using ImageJ software (version 1.54f; National Institutes of Health, Bethesda, MD, USA). The Alizarin Red-positive mineralized area was measured in each field and the mean of the five fields was used as the animal-level value for statistical analysis.

Statistical analysis

Statistical analysis was performed using SPSS 26.0. Data are presented as mean ± standard deviation (SD). Normality was assessed using the Shapiro-Wilk test and homogeneity of variance was assessed using Levene's test. For outcomes meeting these assumptions, one-way analysis of variance (ANOVA) was used to compare the five groups. The variables analyzed by one-way ANOVA were the Lane-Sandhu radiographic score; the RT-qPCR relative expression levels of Runx2, Osterix, PINP, Bax and Caspase-3; Western blot densitometric values for the same five proteins; immunohistochemistry-positive area for the same five proteins; and the Alizarin Red-positive mineralized area. When the omnibus ANOVA was significant, Tukey's honestly significant difference (HSD) post hoc test was applied for pairwise comparisons among the five groups. All tests were two-sided and $p<0.05$ was considered statistically significant.

RESULTS

Radiographic findings and Lane-Sandhu scores

Radiographic findings at 2 weeks post-fracture showed greater callus formation and a less distinct fracture line in the high-dose Compound Miao medicine Jiuxian Luohan bone-setting decoction group than in the model group. Fracture alignment and Kirschner-wire position were acceptable in all groups. Lane-Sandhu scores differed significantly among the five groups (one-way ANOVA: $F = 26.091$, $p < 0.001$). Tukey HSD post hoc comparisons showed that the medium-dose, high-dose and orthopedic bone-setting tablet groups had higher radiographic scores than the model group (all $p<0.01$). In contrast, the low-dose group did not differ statistically from the model group. The high-dose and orthopedic bone-setting tablet groups had the same observed mean score (2.80 ± 0.4472). (Table 3; Fig. 1).

Table 3: Radiographic findings of fracture healing after fracture (mean ± SD, n=5).

Group	N	Fracture healing score	F	*p*-value
Model group	5	0.60 ± 0.5477	26.091	<0.001
Low-dose group	5	0.80 ± 0.4472		
Medium-dose group	5	2.20 ± 0.4472**		
Orthopedic bone-setting tablets	5	2.80 ± 0.4472**		
High-dose group	5	2.80 ± 0.4472**		

Note: **p<0.01 versus the model group according to Tukey's HSD post hoc test. Higher Lane-Sandhu scores indicate more advanced radiographic healing, whereas lower scores indicate little or no callus formation or union.

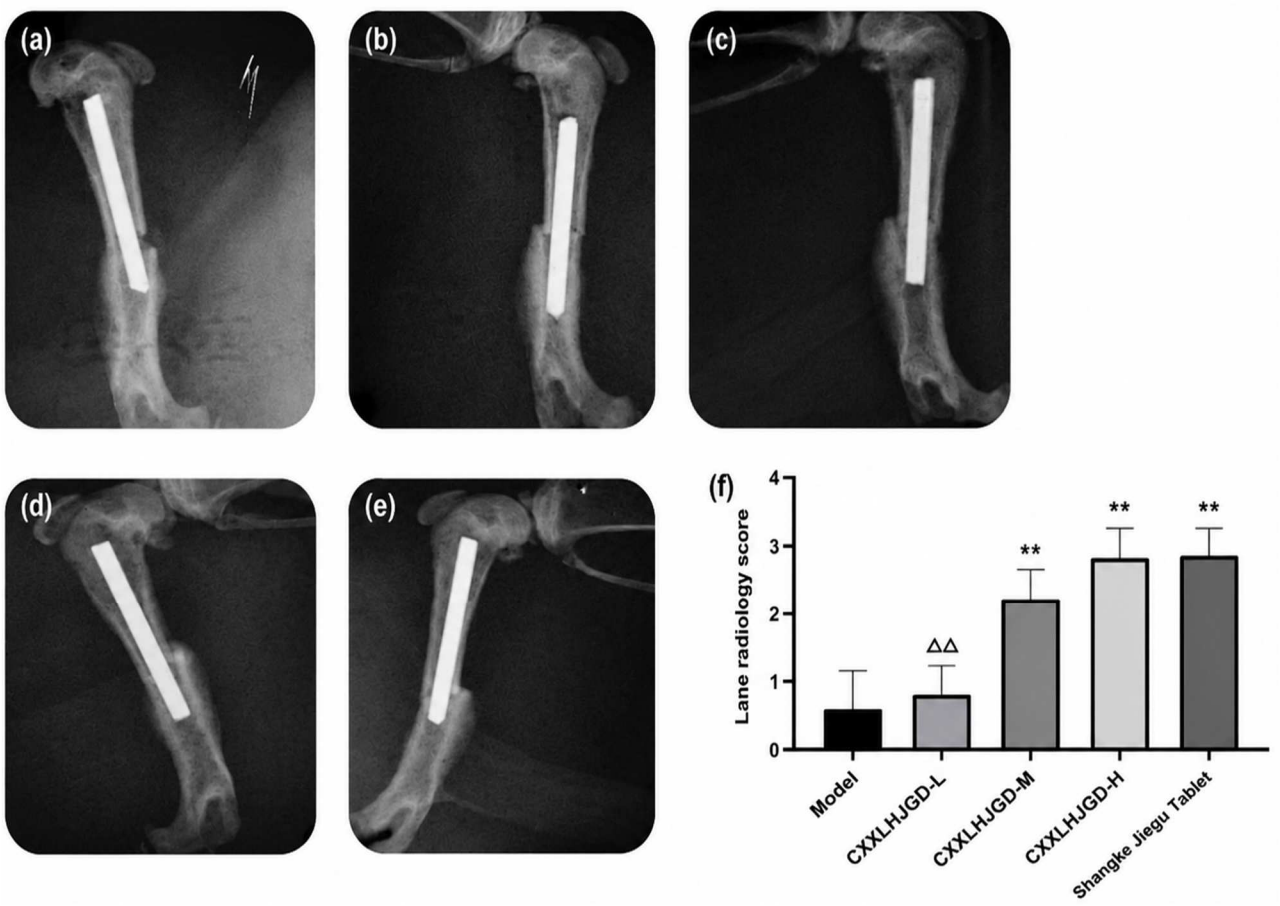

Fig. 1: X-ray images and radiographic scores showing fracture healing after injury. (a) model group; (b) low-dose group; (c) medium-dose group; (d) high-dose group; (e) Orthopedic bone-setting tablet group; (f) Lane radiology scores. *p<0.05 and **p<0.01 indicate comparisons with the model group, whereas △p<0.05 and △△p<0.01 indicate comparisons with the orthopedic bone-setting tablet group.

mRNA expression of Runx2, Osterix, PINP, Bax and Caspase-3

RT-qPCR analysis showed that, compared with the model group, Bax and Caspase-3 mRNA expression decreased in the medium-dose, high-dose and orthopedic bone-setting tablet groups, whereas Runx2, Osterix and PINP mRNA expression increased, particularly in the high-dose group. These findings indicate an osteogenic expression profile accompanied by lower expression of apoptosis-related mRNA markers at the fracture site (Fig. 2).

Western blot protein expression of Runx2, Osterix, PINP, Bax and Caspase-3

Western blot analysis showed increased Runx2, Osterix and PINP protein expression and decreased Bax and Caspase-3 protein expression in decoction-treated groups compared with the model group. The response was most pronounced in the high-dose group, consistent with the RT-qPCR findings (Fig. 3).

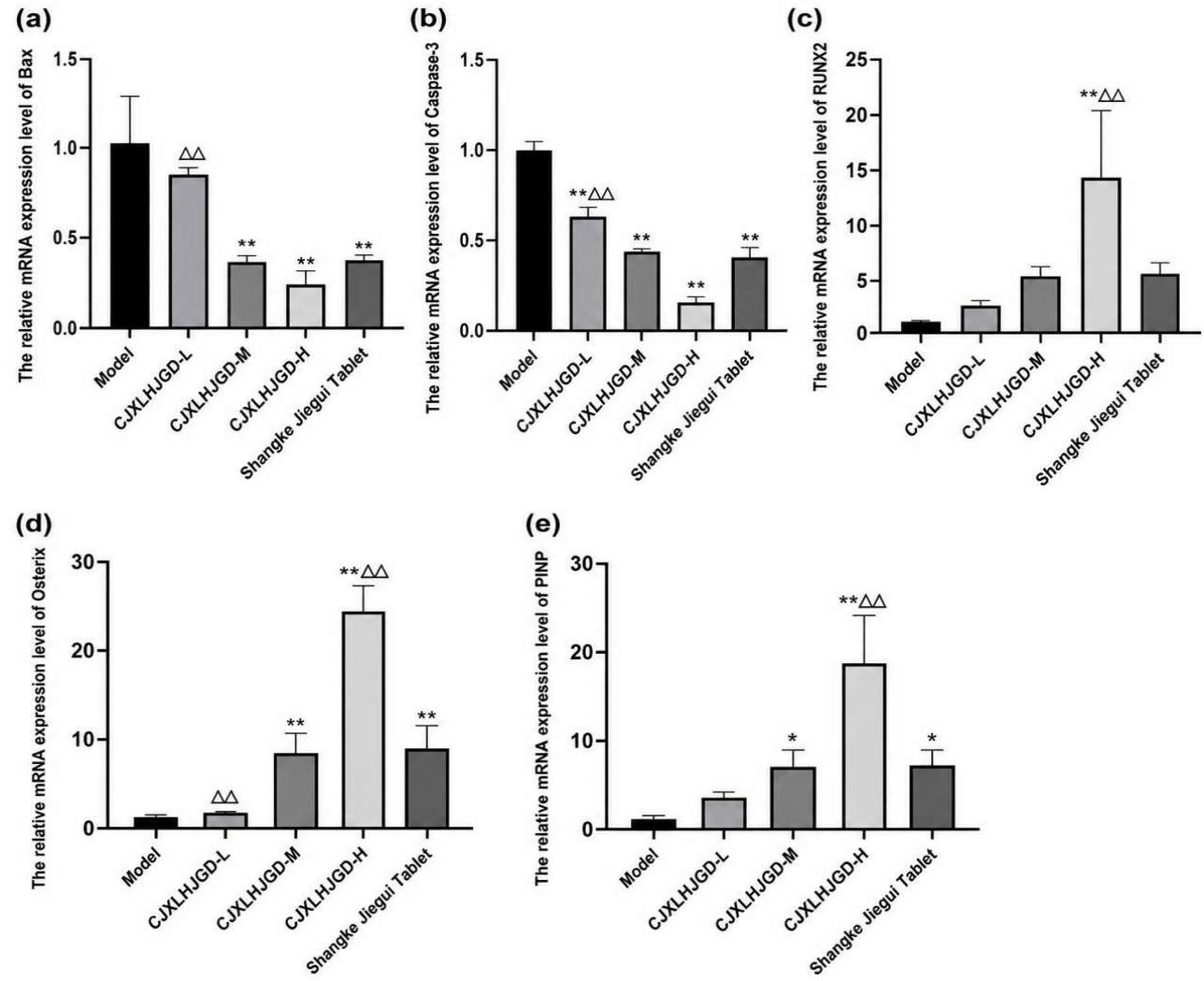

Fig. 2: RT-qPCR analysis of (a) Bax, (b) Caspase-3, (c) Runx2, (d) Osterix and (e) PINP mRNA expression in the model, low-dose, medium-dose, high-dose and orthopedic bone-setting tablet groups. Relative mRNA expression was normalized to ACTB and calculated using the $2^{-\Delta\Delta Ct}$ method. Data are presented as mean ± SD (n=5 rats per group).*p<0.05 and **p<0.01 indicate comparisons with the model group, whereas △p<0.05 and △△p<0.01 indicate comparisons with the orthopedic bone-setting tablet group.

Immunohistochemical protein expression of Runx2, Osterix, PINP, Bax and Caspase-3

Immunohistochemistry demonstrated stronger positive staining for Runx2, Osterix and PINP and weaker positive staining for Bax and Caspase-3 in treated groups compared with the model group. Representative images and quantitative analyses are shown for Runx2 (Fig. 4), Osterix (Fig. 5), PINP (Fig. 6), Bax (Fig. 7) and Caspase-3 (Fig. 8).

Alizarin red staining results

Alizarin Red staining of fracture-site tissue sections showed a larger positively stained mineralized area in the decoction-treated groups than in the model group, with the largest area observed in the high-dose group (Fig. 9). Because the assay was performed on tissue sections, the outcome was the Alizarin Red-positive mineralized area averaged across five fields per animal rather than a count of calcified nodules.

DISCUSSION

Fractures can cause pain, swelling and bleeding. In this rat femoral fracture model, Compound Miao medicine Jiuxian Luohan bone-setting decoction was associated with improved radiographic healing, particularly at the high dose. The Lane-Sandhu score increased from 0.60 ± 0.5477 in the model group to 2.80 ± 0.4472 in the high-dose group, consistent with greater callus formation by week 2. Early callus formation and mineralized matrix deposition are established features of successful fracture repair (Einhorn and Gerstenfeld, 2015; Bahney *et al*., 2019).

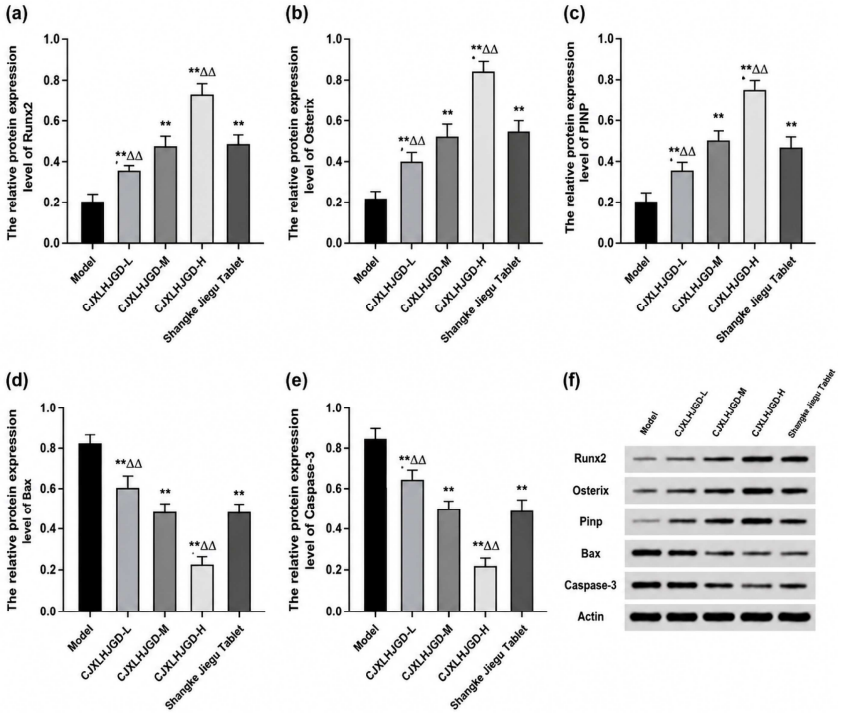

Fig. 3: Western blot densitometric analysis of (a) Runx2, (b) Osterix, (c) PINP, (d) Bax and (e) Caspase-3 protein expression and (f) representative Western blot bands of Runx2, Osterix, PINP, Bax, Caspase-3 and β-actin in the five experimental groups. Target-protein band intensities were normalized to β-actin.Data are presented as mean ± SD (n=5 rats per group).*p<0.05 and **p<0.01 indicate comparisons with the model group, whereas △p<0.05 and △△p<0.01 indicate comparisons with the orthopedic bone-setting tablet group.

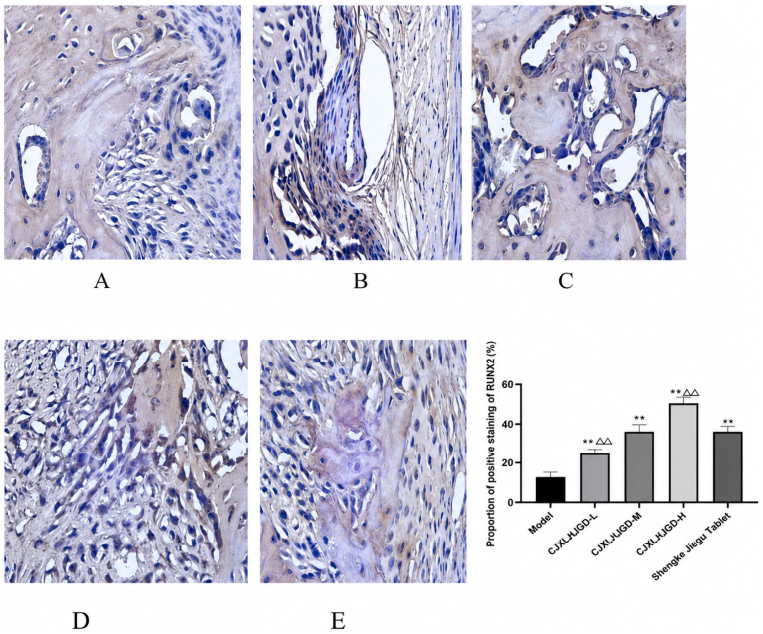

Fig. 4: Representative immunohistochemical images (×400) are shown for the (a) model group, (b) low-dose decoction group, (c) medium-dose decoction group, (d) high-dose decoction group and (e) orthopedic bone-setting tablet group; (f) quantitative analysis of the percentage of Runx2-positive staining area. DAB-positive immunoreactivity appears brown-yellow, whereas hematoxylin-counterstained nuclei appear blue. Data are presented as mean ± SD (n=5 rats per group).*p<0.05 and **p<0.01 indicate comparisons with the model group, whereas △p<0.05 and △△p<0.01 indicate comparisons with the orthopedic bone-setting tablet group.

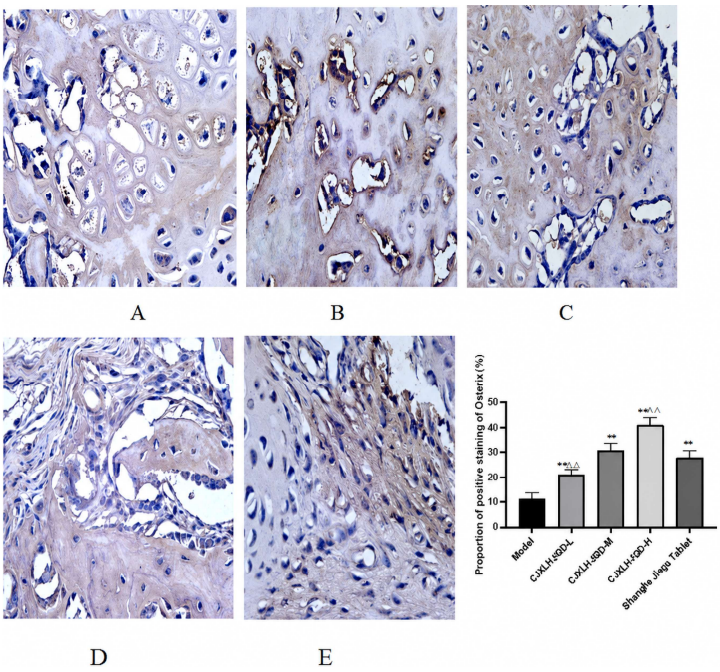

Fig. 5: Representative immunohistochemical images (×400) are shown for the (a) model group, (b) low-dose decoction group, (c) medium-dose decoction group, (d) high-dose decoction group and (e) orthopedic bone-setting tablet group and (f) quantitative analysis of the percentage of Osterix-positive staining area. DAB-positive immunoreactivity appears brown-yellow, whereas hematoxylin-counterstained nuclei appear blue. Data are presented as mean ± SD (n=5 rats per group).*p<0.05 and **p<0.01 indicate comparisons with the model group, whereas △p<0.05 and △△p<0.01 indicate comparisons with the orthopedic bone-setting tablet group.

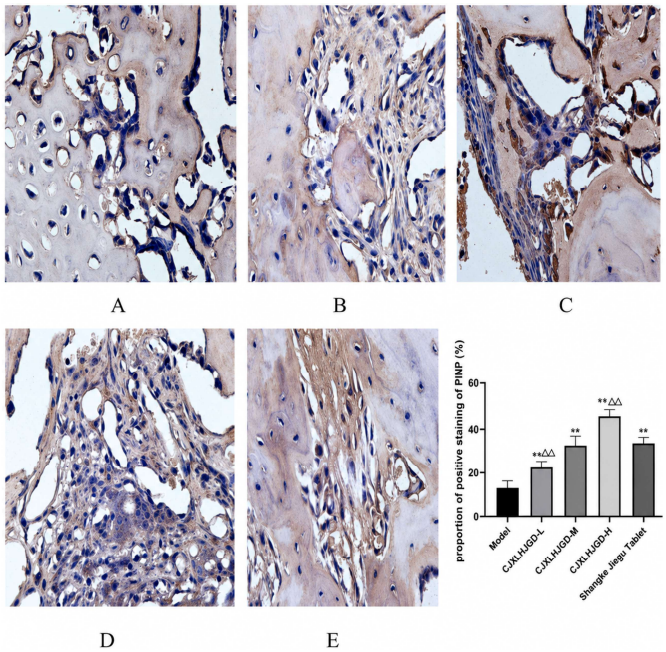

Fig. 6: Representative immunohistochemical images (×400) are shown for the (a) model group, (b) low-dose decoction group, (c) medium-dose decoction group, (d) high-dose decoction group and (e) orthopedic bone-setting tablet group and (f) quantitative analysis of the percentage of PINP-positive staining area. DAB-positive immunoreactivity appears brown-yellow, whereas hematoxylin-counterstained nuclei appear blue. Data are presented as mean ± SD (n=5 rats per group).*p<0.05 and **p<0.01 indicate comparisons with the model group, whereas △p<0.05 and △△p<0.01 indicate comparisons with the orthopedic bone-setting tablet group.

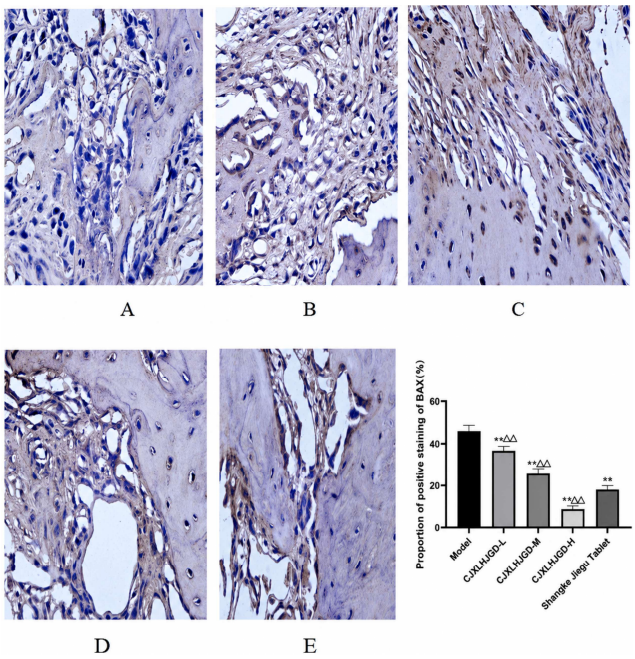

Fig. 7: Representative immunohistochemical images (×400) are shown for the (a) model group, (b) low-dose decoction group, (c) medium-dose decoction group, (d) high-dose decoction group and (e) orthopedic bone-setting tablet group and (f) quantitative analysis of the percentage of Bax-positive staining area. DAB-positive immunoreactivity appears brown-yellow, whereas hematoxylin-counterstained nuclei appear blue. Data are presented as mean ± SD (n=5 rats per group).*p<0.05 and **p<0.01 indicate comparisons with the model group, whereas △p<0.05 and △△p<0.01 indicate comparisons with the orthopedic bone-setting tablet group.

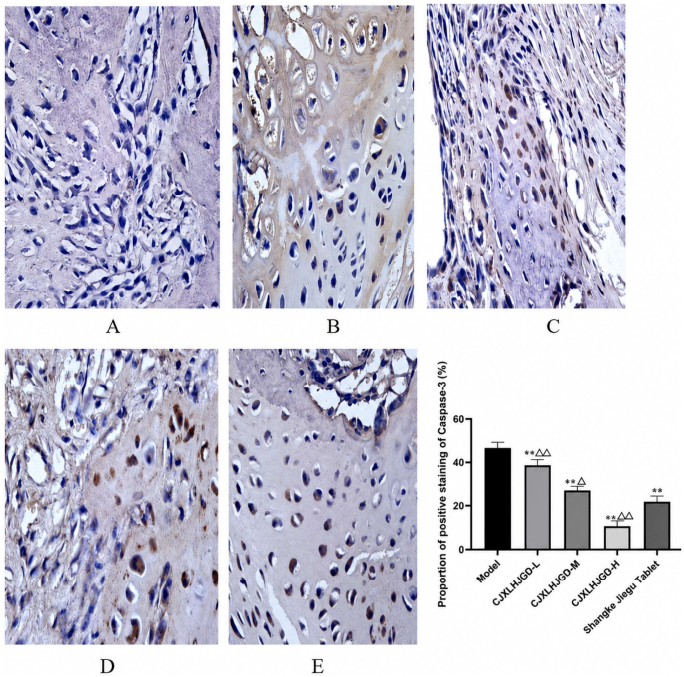

Fig. 8: Representative immunohistochemical images (×400) are shown for the (a) model group, (b) low-dose decoction group, (c) medium-dose decoction group, (d) high-dose decoction group and (e) orthopedic bone-setting tablet group and (f) quantitative analysis of the percentage of Caspase-3-positive staining area. DAB-positive immunoreactivity appears brown-yellow, whereas hematoxylin-counterstained nuclei appear blue. Data are presented as mean ± SD (n=5 rats per group).*p<0.05 and **p<0.01 indicate comparisons with the model group, whereas △p<0.05 and △△p<0.01 indicate comparisons with the orthopedic bone-setting tablet group.

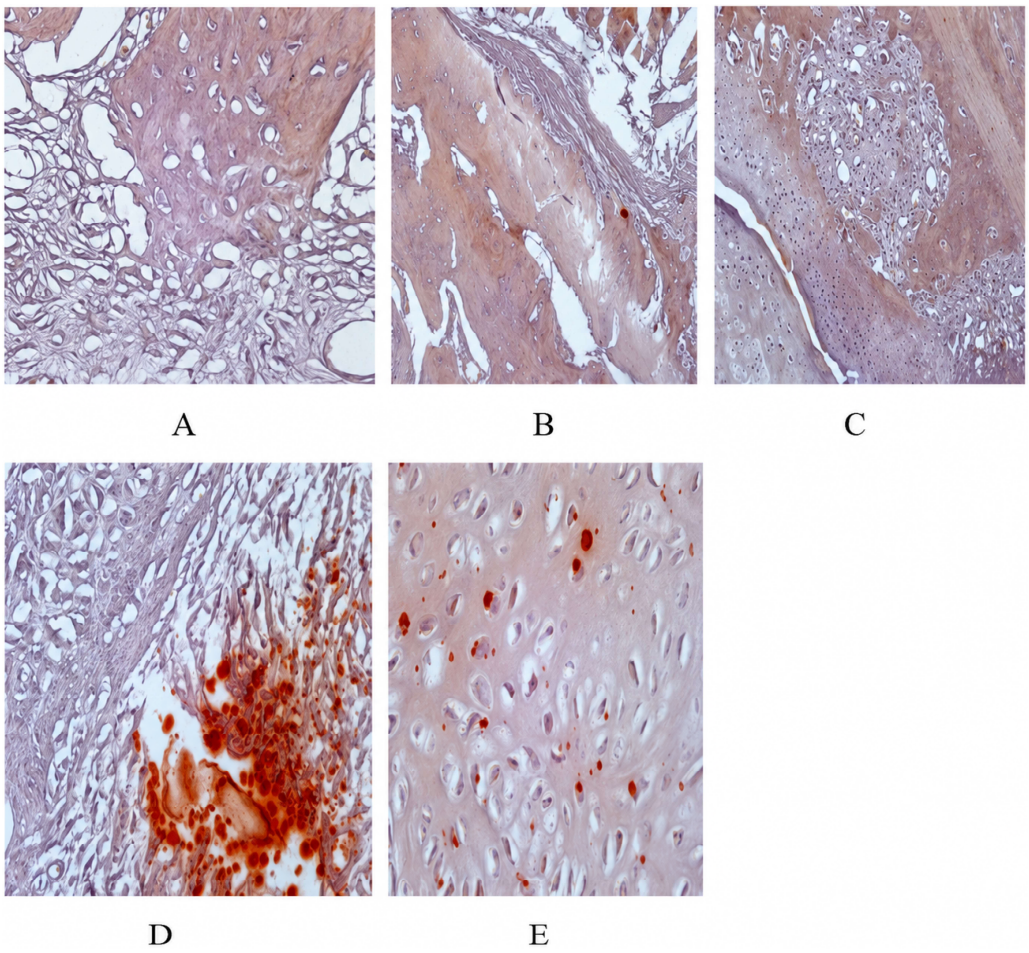

Fig. 9: Representative Alizarin Red-stained sections are shown for the (a) model group, (b) low-dose Compound Miao medicine Jiuxian Luohan bone-setting decoction group, (c) medium-dose decoction group, (d) high-dose decoction group and (e) orthopedic bone-setting tablet group.*p<0.05 and **p<0.01 indicate comparisons with the model group, whereas △p<0.05 and △△p<0.01 indicate comparisons with the orthopedic bone-setting tablet group.

The molecular findings showed increased expression of the osteogenic markers Runx2, Osterix and PINP after treatment. Runx2 and Osterix regulate osteoblast differentiation, whereas PINP reflects type I collagen formation and bone-matrix synthesis. These observations are consistent with evidence that osteoblast differentiation is critical for bone formation and fracture repair (Ponzetti and Rucci, 2021; Chan *et al*., 2021; Qin *et al*., 2021). The higher expression of these markers in the high-dose group therefore supports a potential enhancement of osteogenic activity at the fracture site.

The treated groups also showed reduced expression of Bax and Caspase-3, two apoptosis-related markers. Apoptosis-related pathways can influence skeletal-cell survival and bone remodeling (Obeng, 2021; Sahoo *et al*., 2023). However, apoptosis was not measured directly by TUNEL staining, Annexin V/PI flow cytometry, cleaved Caspase-3 immunostaining or lineage-specific assays. Accordingly, the present findings demonstrate an association between treatment and reduced expression of apoptosis-related markers but do not establish that inhibition of osteoblast apoptosis is the causal mechanism underlying improved fracture healing.

This study has several limitations. The experiment used a relatively small sample and included only male rats, which may limit generalizability. Fracture repair was assessed at a limited number of time points, preventing full characterization of the dynamic inflammatory, reparative, mineralization and remodeling phases. In addition, apoptosis was inferred from Bax and Caspase-3 expression rather than measured directly. Further studies should incorporate direct apoptosis assays, cell-specific validation, biomechanical testing, longer follow-up and standardized quality control of the herbal preparation.

CONCLUSION

Compound Miao medicine Jiuxian Luohan bone-setting decoction was associated with improved radiographic fracture healing and favorable changes in osteogenic markers (Runx2, Osterix and PINP) and apoptosis-related markers (Bax and Caspase-3) in a rat femoral fracture

model. The findings suggest that the decoction may contribute to fracture repair through enhanced osteogenic activity and altered apoptosis-related signaling; however, causality and cell-specific mechanisms remain to be confirmed. Future research should include non-fractured sham controls, multiple time points, direct apoptosis assays, cell-specific validation, larger sample sizes, standardized herbal quality control and complete source-data reporting.

Acknowledgements
This work was supported by the Qiankehe Foundation-ZK[2024] General 414. The authors gratefully acknowledge Guizhou University of Traditional Chinese Medicine for providing research facilities. Animal experiments were conducted at the Animal Research Institute, Huaxi Campus, Guizhou University of Traditional Chinese Medicine.

Authors' contributions
Haoran Wan: Designed and performed the experimental research and drafted the manuscript; Zhengxing Xie, Lingcheng Deng, Liang Yu, Zhong Ning, Hongfa Wang, Jiabao Zheng and Shaoyang Zhai: Contributed to experiment implementation, data collection and analysis; Lianghua Tang: Supervised the overall research, secured funding and critically reviewed and revised the manuscript. All authors read and approved the final version of the manuscript.

Funding
This study was funded by the Qiankehe Foundation-ZK[2024] General 414.

Data availability statement
The datasets generated during and/or analyzed during the current study are available from the corresponding author on reasonable request.

Ethical approval
All animal experiments were approved by the Animal Ethics Committee of Guizhou University of Traditional Chinese Medicine (approval no. 2024005). The study was conducted in accordance with institutional animal welfare guidelines and relevant regulations. This study was performed in adherence with the ARRIVE guidelines. See supplementary file for the ARRIVE checklist.

Conflict of interest
The authors declare no conflict of interest.

Supplementary data
https://pjps.pk/uploads/2026/09/SUP1788605504.pdf

REFERENCES

Bahney CS, Zondervan RL, Allison P, Theologis A, Ashley JW, Ahn J, Miclau T, Marcucio RS and Hankenson KD (2019). Cellular biology of fracture healing. *J. Orthop. Res.*, **37**(1): 35-50.

Beltran MJ, Collinge CA and Gardner MJ (2016). Stress modulation of fracture fixation implants. *J. Am. Acad. Orthop. Surg.*, **24**(10): 711-719.

Bustin SA, Benes V, Garson JA, Hellemans J, Huggett J, Kubista M, Mueller R, Nolan T, Pfaffl MW, Shipley GL, Vandesompele J and Wittwer CT (2009). The MIQE guidelines: Minimum information for publication of quantitative real-time PCR experiments. *Clin. Chem.*, **55**(4): 611-622.

Chacon EL, Bertolo MRV, de Guzzi Plepis AM, da Conceicao Amaro Martins V, Dos Santos GR, Pinto CAL, Pelegrine AA, Teixeira ML, Buchaim DV, Nazari FM, Buchaim RL, Sugano GT and da Cunha MR (2023). Collagen-chitosan-hydroxyapatite composite scaffolds for bone repair in ovariectomized rats. *Sci. Rep.*, **13**(1): 28.

Chan WCW, Tan Z, To MKT and Chan D (2021). Regulation and role of transcription factors in osteogenesis. *Int. J. Mol. Sci.*, **22**(11): 5445.

Chavassieux P, Portero-Muzy N, Roux JP, Garnero P and Chapurlat R (2015). Are biochemical markers of bone turnover representative of bone histomorphometry in 370 postmenopausal women? *J. Clin. Endocrinol. Metab.*, **100**(12): 4662-4668.

Chen JH, Lin X, Bu C and Zhang X (2018). Role of advanced glycation end products in mobility and considerations in possible dietary and nutritional intervention strategies. *Nutr. Metab.*, **15**: 72.

Dai DF, Chiao YA, Marcinek DJ, Szeto HH and Rabinovitch PS (2014). Mitochondrial oxidative stress in aging and healthspan. *Longev. Healthspan.*, **3**: 6.

Einhorn TA and Gerstenfeld LC (2015). Fracture healing: Mechanisms and interventions. *Nat. Rev. Rheumatol.*, **11**(1): 45-54.

Fernandes JB, Ferreira N, Domingos J, Ferreira R, Amador C, Pardal N, Castro C, Simoes A, Fernandes S, Bernardes C, Vareta DA, Pecas D, Ladislau D, Sousa N, Duarte A and Godinho C (2023). Health professionals' motivational strategies to enhance adherence in the rehabilitation of people with lower limb fractures: Scoping review. *Int. J. Environ. Res. Public Health*, **20**(22): 7050.

Fu H, Doll B, McNelis T and Hollinger JO (2007). Osteoblast differentiation *in-vitro* and *in-vivo* promoted by Osterix. *J. Biomed. Mater. Res. A*, **83**(3): 770-778.

Hou C, Wang X, Jiang W, Bian Z, Zhu L and Li M (2021). Peptide 11R-VIVIT promotes fracture healing in osteoporotic rats. *Int. J. Mol. Med.*, **48**(2): 162.

Jayankura M, Schulz AP, Delahaut O, Witvrouw R, Seefried L, Berg BV, Heynen G and Sonnet W (2021). Percutaneous administration of allogeneic bone-forming

cells for the treatment of delayed unions of fractures: A pilot study. *Stem Cell Res. Ther.*, **12**(1): 363.

Lane JM and Sandhu HS (1987). Current approaches to experimental bone grafting. *Orthop. Clin. North Am*., **18**(2): 213-225.

Li Z, Wang W, Xu H, Ning Y, Fang W, Liao W, Zou J, Yang Y and Shao N (2017). Effects of altered CXCL12/CXCR4 axis on BMP2/Smad/Runx2/Osterix axis and osteogenic gene expressions during osteogenic differentiation of MSCs. *Am. J. Transl. Res.*, **9**(4): 1680-1693.

Luo TD, Ashraf A, Larson AN, Stans AA, Shaughnessy WJ and McIntosh AL (2015). Complications in the treatment of adolescent clavicle fractures. *Orthopedics*, **38**(4): e287-e291.

MalekiGorji M, Golestaneh A and Razavi SM (2020). The effect of two phosphodiesterase inhibitors on bone healing in mandibular fractures. *J. Korean Assoc. Oral Maxillofac. Surg.*, **46**(4): 258-265.

Moon YJ, Yun CY, Choi H, Kim JR, Park BH and Cho ES (2018). Osterix regulates corticalization for longitudinal bone growth via integrin beta3 expression. *Exp. Mol. Med.*, **50**(7): 1-11.

Obeng E (2021). Apoptosis (programmed cell death) and its signals - A review. *Braz. J. Biol.*, **81**(4): 1133-1143.

Percie du Sert N, Hurst V, Ahluwalia A, Alam S, Avey MT, Baker M, Browne WJ, Clark A, Cuthill IC, Dirnagl U, Emerson M, Garner P, Holgate ST, Howells DW, Karp NA, Lazic SE, Lidster K, MacCallum CJ, Macleod M, Pearl EJ, Petersen OH, Rawle F, Reynolds P, Rooney K, Sena ES, Silberberg SD, Steckler T and Würbel H (2020). The ARRIVE guidelines 2.0: Updated guidelines for reporting animal research. *PLoS Biol*., **18**(7): e3000410.

Ponzetti M and Rucci N (2021). Osteoblast differentiation and signaling: Established concepts and emerging topics. *Int. J. Mol. Sci.*, **22**(13): 6651.

Qin X, Jiang Q, Komori H, Sakane C, Fukuyama R, Matsuo Y, Ito K, Miyazaki T and Komori T (2021). Runx2 is required for bone matrix protein gene expression in committed osteoblasts in mice. *J. Bone Miner. Res.*, **36**(10): 2081-2095.

Ramazzotti G, Fiume R, Chiarini F, Campana G, Ratti S, Billi AM, Manzoli L, Follo MY, Suh PG, McCubrey J, Cocco L and Faenza I (2019). Phospholipase C-beta1 interacts with cyclin E in adipose-derived stem cells osteogenic differentiation. *Adv. Biol. Regul.*, **71**: 1-9.

Reagan-Shaw S, Nihal M and Ahmad N (2008). Dose translation from animal to human studies revisited. *FASEB J*., **22**(3): 659-661.

Ren C, Xu Y, Liu H, Wang Z, Ma T, Li Z, Sun L, Huang Q, Zhang K, Zhang C, Cui Y, Wang Q and Lu Y (2022). Effects of RUNX2 on the autophagy of rapamycin-treated osteoblasts. *Bioengineered*, **13**(3): 5262-5276.

Ren L, Zhu X, Tan J, Lv X, Wang J and Hua F (2023). MiR-210 promotes bone formation in ovariectomized rats by regulating osteogenic/adipogenic differentiation of bone marrow mesenchymal stem cells through downregulation of EPHA2. *J. Orthop. Surg. Res.*, **18**(1): 811.

Rodriguez-Gonzalez J and Gutierrez-Kobeh L (2023). Apoptosis and its pathways as targets for intracellular pathogens to persist in cells. *Parasitol. Res.*, **123**(1): 60.

Sahoo G, Samal D, Khandayataray P and Murthy MK (2023). A review on caspases: Key regulators of biological activities and apoptosis. *Mol. Neurobiol.*, **60**(10): 5805-5837.

Suzuki A, Minamide M, Iwaya C, Ogata K and Iwata J (2020). Role of metabolism in bone development and homeostasis. *Int. J. Mol. Sci.*, **21**(23): 8992.

Toosi S, Behravan N and Behravan J (2018). Nonunion fractures, mesenchymal stem cells and bone tissue engineering. *J. Biomed. Mater. Res. A*, **106**(9): 2552-2562.

Uenaka M, Yamashita E, Kikuta J, Morimoto A, Ao T, Mizuno H, Furuya M, Hasegawa T, Tsukazaki H, Sudo T, Nishikawa K, Okuzaki D, Motooka D, Kosaka N, Sugihara F, Boettger T, Braun T, Ochiya T and Ishii M (2022). Osteoblast-derived vesicles induce a switch from bone-formation to bone-resorption *in-vivo*. *Nat. Commun.*, **13**(1): 1066.

Wang B, Shi Z, Li D and Yu J (2025). Predictive model of delayed union of tibial and fibular fractures based on PGC-1alpha, NOS and Runx2. *Eur. J. Med. Res.*, **30**(1): 978.

Yin N, Zhu L, Ding L, Yuan J, Du L, Pan M, Xue F and Xiao H (2019). MiR-135-5p promotes osteoblast differentiation by targeting HIF1AN in MC3T3-E1 cells. *Cell Mol. Biol. Lett.*, **24**: 51.

Zhang Y, Lin Y, Xiao L, Feng E, Wang W and Lin L (2015). The effects of icariine concentration on osteoclasts bone resorption induced by titanium particles *in-vitro*. *Regen. Biomater.*, **2**(3): 197-202.

Zhang Y, Xu J, Ruan YC, Yu MK, O'Laughlin M, Wise H, Chen D, Tian L, Shi D, Wang J, Chen S, Feng JQ, Chow DH, Xie X, Zheng L, Huang L, Huang S, Leung K, Lu N, Zhao L, Li H, Zhao D, Guo X, Chan K, Witte F, Chan HC, Zheng Y and Qin L (2016). Implant-derived magnesium induces local neuronal production of CGRP to improve bone-fracture healing in rats. *Nat. Med.*, **22**(10): 1160-1169.